J. Geogr. Sci. 2018, 28(9): 1341-1368
DOI: https://doi.org/10.1007/s11442-018-1529-2

Spatiotemporal characteristics of seasonal precipitation and their relationships with ENSO in Central Asia during 1901–2013

CHEN Xi[1], WANG Shanshan[2], HU Zengyun[1,3], ZHOU Qiming[3], HU Qi[4]

1. State Key Laboratory of Desert and Oasis Ecology, Xinjiang Institute of Ecology and Geography, CAS, Urumqi 830011, China;
2. Key Open Laboratory of Arid Climate Change and Disaster Reduction of CMA, Institute of Arid Meteorology, CMA, Lanzhou 730000, China;
3. Department of Geography, Hong Kong Baptist University, Kowloon Tong, Kowloon, Hong Kong, China;
4. School of Natural Resources and Department of Earth and Atmospheric Sciences, University of Nebraska–Lincoln, Lincoln, Nebraska

Abstract: The vulnerable ecosystem of the arid and semiarid region in Central Asia is sensitive to precipitation variations. Long-term changes of the seasonal precipitation can reveal the evolution rules of the precipitation climate. Therefore, in this study, the changes of the seasonal precipitation over Central Asia have been analyzed during the last century (1901–2013) based on the latest global monthly precipitation dataset Global Precipitation Climatology Centre (GPCC) Full Data Reanalysis Version 7, as well as their relations with El Niño-Southern Oscillation (ENSO). Results show that the precipitation in Central Asia is mainly concentrated in spring and summer seasons, especially in spring. For the whole study period, increasing trends were found in spring and winter, while decreasing trends were detected in summer and fall. Inter-annual signals with 3–7 years multi-periods were derived to explain the dominant components for seasonal precipitation variability. In terms of the dominant spatial pattern, Empirical orthogonal function (EOF) results show that the spatial distribution of EOF-1 mode in summer is different from those of the other seasons during 1901–2013. Moreover, significant ENSO-associated changes in precipitation are evident during the fall, winter, spring, and absent during summer. The lagged associations between ENSO and seasonal precipitation are also obtained in Central Asia. The ENSO-based composite analyses show that these water vapor fluxes of spring, fall and winter precipitation are mainly generated in Indian and North Atlantic Oceans during El Niño. The enhanced westerlies strengthen the western water vapor path for Central Asia, thereby causing a rainy winter.

Keywords: Central Asia; seasonal precipitation; spatiotemporal pattern; ENSO

Received: 2018-01-05 **Accepted:** 2018-03-20
Foundation: International Cooperation Fund of Ecological Effects of Climate Change and Land Use/Cover Change in Arid and Semiarid Regions of Central Asia in the Most Recent 500 Years, No.41361140361; The Western Scholars of the Chinese Academy of Sciences, No.2015-XBQN-B-20; National Natural Science Foundation of China, No.41471340, No.41605055; Hong Kong Baptist University Faculty Research, No.FRG2/17-18/030
Author: Chen Xi, Professor, specialized in hydrology and water resource, as well as environmental remote sensing.
E-mail: chenxi@ms.xjb.ac.cn

1 Introduction

The variations of seasonal precipitation are widely regarded as key indicators of climate variations (Sorg *et al*., 2012; Chou *et al*., 2013; Bintanja and Selten, 2014). And these changes of precipitation in both space and time have significant influences on the spatio-temporal distributions of water resources and result in floods or droughts, which will impact on the natural ecosystem and human society seriously (Smith *et al*., 2012; Chou *et al*., 2013). Under the global warming, the seasonal precipitation has been experienced large changes at regional and global scales, such as the increase in the range between wet and dry season precipitation (Chou *et al*., 2013). Therefore, it is urgent and necessary to explore the spatio-temporal changes of the seasonal precipitation.

Recently, more and more attention has been focused on the variations of the seasonal precipitation by observed datasets (e.g. Aizen and Aizen, 1997; Hu, 1997; Zveryaev, 2004; Wang and Zhou 2005; Zhang *et al*., 2011; Rudolph and Friedrich 2013) and climate models (e.g. Hu *et al*., 2003; Russo and Sterl, 2012; Maussion *et al*., 2014). During 1952–1999, increased seasonal precipitation is examined over northern mid to high latitudes from observed datasets and simulated models (Noake *et al*., 2012). For the period of 1979–2010, the wet seasons become much wetter and dry seasons become much drier, and this tendency is also obtained using a number of global observational datasets (Chou *et al*., 2013). The seasonal rainfall patterns between China, Korea and Japan are different, and the 850 hPa circulation controlled the seasonal rainfall oscillation in Korea, eastern China and Japan (Qian *et al*., 2002). Over China, the increasing trend of winter precipitation occurred in most of China and northwest China experienced the increasing trends in all seasons during the past half century (Wang and Zhou, 2005; Wang and Yan, 2009; Zhang *et al*., 2011). Large spatial difference with the summer precipitation climatology and variability lower than those of winter precipitation were founded over Eastern Europe during 1958–1998 (Zveryaev, 2004).

El Niño-Southern Oscillation (ENSO) is the most dominant inter-annual signal of climate variability on Earth, and is known to influence the climate changes at the regional and global scales through the atmosphere-ocean coupling (Ropelewski and Halpert, 1987; Dai *et al*., 1997; Xie and Arkin 1997; Ward *et al*., 2014; Emerton *et al*., 2017). Particularly, previous studies (Dai and Wigley 2000; Chen *et al*., 2017; Dai and Arkin 2017; Jia and Ge 2017) pointed out that ENSO plays very important roles on the variability, magnitude, and distributions of the seasonal precipitation. Dai and Wigley (2000) reported that the ENSO-induced precipitation have different patterns at different seasons which are related to large-scale atmospheric circulation changes caused by sea surface temperature (SST) and wind anomalies. The spring precipitation of Europe is strongly influenced by ENSO (Hughes and Saunders 2002), while summer and winter precipitation are associated with the North Atlantic Oscillation (NAO) (Zveryaev, 2004). Some ENSO-related changes in storm activity are also evident during fall and winter over Europe. These seasonal teleconnections over Europe appear to be mediated by the changes in upper tropospheric conditions along the coast of Europe which produce onshore or offshore moisture flux anomalies (Shaman, 2014). The circulation anomaly induced by warming in the tropical Indian Ocean enhances the relationship between ENSO and summer precipitation over northeastern China (Han *et al*., 2017). ENSO also has large impacts on the seasonal at different timescales, such as the transition seasons over the southwest Central Asia (Mariotti, 2007), the intra-seasonal precipitation over southwestern Asia (Hoell *et al.*, 2012, 2015; 2017) and the inter-decadal changes of the winter precipitation over China (Jia and Ge, 2017).

As one of the largest arid and semiarid regions, Central Asia has experienced rising temperature and increased precipitation during the last century (Hu *et al.*, 2014; Hu *et al.*, 2016b; Hu *et al.*, 2017). The changes of the precipitation have large influences on the ecosystem over this arid and semiarid region (Hu *et al.*, 2014). Although some studies are applied on precipitation over Central Asia (Aizen *et al.*, 2001; Schiemann *et al.*, 2008; Chen *et al.*, 2011; Hu *et al.*, 2016a, 2016b), the spatiotemporal analysis of the seasonal precipitation is limited. For example, whether the seasonal precipitation has increased trend during the last century, and among the four seasons which one has the largest change? The annual precipitation has the obvious spatial differences between Xinjiang and the five states of Central Asia (Xu *et al.*, 2015; Hu *et al.*, 2017). Then, whether the differences still existed for the seasonal precipitation. Moreover, what are the relationships between the seasonal precipitation and ENSO over this region?

In order to address the above challenges and complexities, in this study, we systematically examine the evolutions of the seasonal precipitation over Central Asia during the last century. Because of the high ability to capture the temporal variations and spatial patterns of the seasonal precipitation climate over this region (Hu *et al.*, 2018), the latest version of GPCC Full Data Reanalysis Version 7 (GPCC V7) dataset with the period 1901–2013 is adopted as in Hu *et al.* (2017). The first objective is to analyze the temporal features of the seasonal precipitation during 1901–2013, including the linear trend and multi-periods. The spatial features including the spatial distributions of the linear trends and identifying the dominant spatial pattern are explored as the second objective. Since the significantly positive correlation between the annual precipitation and ENSO is obtained (Hu *et al.*, 2017), the third objective is to examine the correlations between the seasonal precipitation and ENSO, and the influence of ENSO on the precipitation is detected through the composite method.

2 Study area, datasets and analysis methods

2.1 Study area

This study area encompasses five countries: Kazakhstan, Kyrgyzstan, Tajikistan, Turkmenistan, Uzbekistan (hereafter ‘CAS5’), and Xinjiang Uygur Autonomous Region of China (Figure 1). This arid and semiarid region is located in the hinterland of the Eurasian continent, and is primarily dominated by the westerly winds (Lioubimtseva and Cole, 2006; Chen and Zhou, 2015). It has been experienced a significant increasing trend of the surface temperature (Hu *et al.*, 2014) and an overall increasing trend of the annual precipitation during the last century (Hu *et al.*, 2017).

2.2 Datasets

The global monthly land-surface precipitation dataset GPCC V7 (Schneider *et al.*, 2015) with a spatial resolution of 0.5°×0.5° for the period 1901–2013 is used (ftp://ftp.dwd.de/pub/

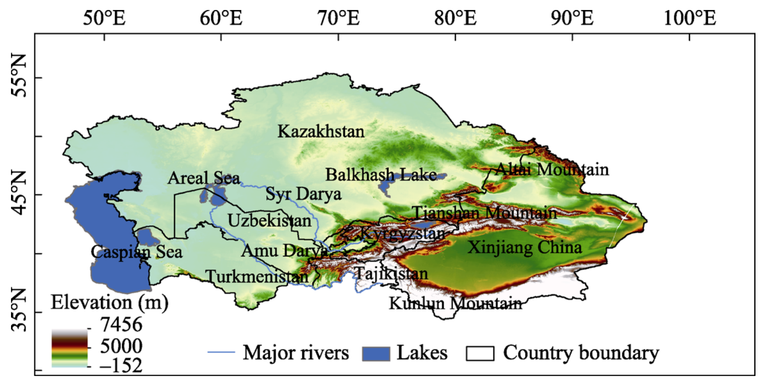

Figure 1 Study area and orographic features in Central Asia

data/gpcc/html/fulldata_v7_doi_download.html). This gridded dataset is based on 75,000 meteorological stations world-wide with record durations of 10 years or longer and it has been widely used to support regional climate monitoring, model validation, climate variability analysis and water resources assessment studies (Becker *et al.*, 2013; Schneider *et al.*, 2014). Recent studies (Hu *et al.*, 2016a; Hu *et al.*, 2017; Hu *et al.*, 2018) also suggest that the correlation coefficient of the annual precipitation between the observed stations over this region and GPCC is larger than 0.88 and the obsolete error is only 5 mm which indicate that this dataset can well describe the spatiotemporal patterns of the precipitation climate over Central Asia.

ENSO is indicated by Niño 3.4 index, derived from SST anomaly estimated in the Niño 3.4 region (5°N–5°S, 120°–170°W). This Niño 3.4 index with the period of 1950 to present is obtained from the Climate Prediction Center of National Oceanic and Atmospheric Administration (NOAA) (http://www.cpc.ncep.noaa.gov/data/indices/ersst4.nino.mth.81-10.ascii). In order to investigate the moisture flux sources and the moisture flux transport paths of the seasonal precipitation over Central Asia, the water vapor flux (vertical integral of eastward water vapor flux and vertical integral of northward water vapor flux), vertical integral of divergence of moisture flux from the monthly ERA-20C with a spatial resolution of 1.0°×1.0° for the period 1900–2010 (Poli *et al.*, 2016) were used (http://apps.ecmwf.int/datasets/data/era20c-moda/). Moreover, the geopotential height (HGT), U component of wind and V component of wind at 200 hPa and 850 hPa levels of ERA-20C were applied to explore the upper and lower tropospheric response to ENSO which can provide a better understanding of the physical mechanisms from the atmospheric circulations.

2.3 Analysis methods

In this study, the four seasons are defined as spring [March-May (MAM)], summer [June-August (JJA)], fall [September-November (SON)] and winter [December-February (DJF)]. Comparing with a previous study on Central Asia annual precipitation (Hu *et al.*, 2017), three periods: 1901–2013, 1951–2013 and 1979–2013 are considered for the temporal variations and spatial patterns of the seasonal precipitation. Since the coefficient of variation (CV) defined as the ratio of the standard deviation (STDV) to the mean can well assessing the variability of the time series and apparently permits the comparison of variates free from scale effects (Brown 1998), therefore, it is used to measure the year to variabilities of the seasonal precipitation. The linear trend K is used to quantify the tendency of the seasonal precipitation which is obtained by the linear least square method and the significance is identified by the Student's *t* test at 95% confidence levels ($p<0.05$).

In order to extract the multi-period characteristics of the seasonal precipitation and the Niño 3.4 index, the Ensemble Empirical Mode Decomposition (EEMD) method (Wu and Huang, 2009; Ji *et al.*, 2014) is applied. For a time series $X(t)$ is decomposed in the instrinsic mode functions (IMFs) and the residue term r. The IMFs display the different multi-periods and r is the nonlinear trend (Ji *et al.*, 2014). The added white noise in each EEMD ensemble member has a standard deviation of 0.2 and an ensemble size of 100 is used. The significance of the periodicity for each EEMD component is detected at a 95% confidence level (Wu and Huang 2004). The detailed description of the EEMD method can be found in Wu and Huang (2009).

The spatiotemporal structures of the long-term variations of seasonal precipitation are examined by the empirical orthogonal function (EOF) analyses (Lorenz, 1956). EOF analyses can identify the dominant spatial pattern according to the spatial mode (EOF mode) and obtain the corresponding time coefficients which explain the magnitude of the variation of each EOF model of the seasonal precipitation. Before the EOF analysis, the annual cycle was removed from all grid point time series by subtracting from each seasonal value the respective season's long-term mean. Following North *et al.* (1982), a significance test is applied to distinguish the physical signal from the noise in the EOF.

Correlation coefficient (CC) values between the inter-annual signals of the seasonal precipitation and ENSO are computed to quantify the inter-annual correlations between the seasonal precipitation and ENSO. According to the definition of Qian *et al.* (2011), the inter-annual signals of ENSO and precipitation are obtained by EEMD method: combining the components with their periods smaller than 10-year as the inter-annual timescale component. CC values are determined by an effective degree of freedom when considering the first-order autocorrelations at 95% and 99% confidence levels (Bretherton *et al.*, 1999). In this study, two types of CC values are defined: the first CC is computed from the time series with the different periods from *i* year (starting year) to 2013. Considering the statistical significance, the starting year *i* is from 1901 to 1984. The second type CC is computed by the 30-yr moving of inter-annual time series between the seasonal precipitation and ENSO (named 30-yr moving CC) which is used to investigate the stable (or robust) of the correlation in time.

At last, the seasonal ENSO-based composite analyses (using El Niño minus La Niña years) are conducted to discuss the possible physical process. In this study, the Niño 3.4 indices are normalized by the mean value and STDV. Then, the El Niño year is defined when the normalized Niño 3.4 indices are not smaller than one STDV and the La Niña is defined as the normalized Niño 3.4 indices are smaller than –STDV (Shaman, 2014; Hu *et al.*, 2017).

3 Results

3.1 Temporal changes over the entire study area (Central Asia)

For 1901–2013, MAM (Mean=59 mm) and JJA (Mean=57 mm) have larger precipitation than SON (Mean=43 mm) and DJF (Mean=41 mm) which indicates that the precipitation mainly occurs in spring and summer over Central Asia, especially in spring (Table 1). The

CV (25%) of SON shows the largest variabilities of the precipitation than those of the other seasons (Table 1 and Figure 2). Figures 2c and 2d show that sharp drops are occurred from 1901 to the early 1940s for SON and DJF, and flowed by a rise till the 1980s which is consistent with the variability of the annual precipitation (Hu *et al*., 2016a). Moreover, positive anomalies of JJA mainly occurred from 1901 to 1970 (Figure 2b). From the 1930s to 1960s, SON and DJF have largely negative anomalies which imply that drought events may occur in these two seasons (Figures 2c and 2d). On the whole, increasing trends are found for MAM and DJF with the values of 0.41 mm/10a and 0.39 mm/10a over Central Asia (Table 1). JJA and SON have slightly decreasing trends.

Table 1 Mean (mm), coefficient of variation (CV: %) and linear trend (K: mm/10a) of the seasonal precipitation over mountainous area, plain area and Central Asia during 1901–2013, 1951–2013 and 1979–2013

Study area	Season	1901–2013			1951–2013			1979–2013		
		Mean	CV	K	Mean	CV	K	Mean	CV	K
Central Asia	MAM	59	21	0.41	61	22	0.49	61	20	0.42
	JJA	57	20	–0.09	57	19	0.4	58	19	1.62
	SON	43	25	–0.1	43	22	0.23	44	21	–1.97
	DJF	41	20	0.39	42	18	0.77	43	17	0.24
Mountainous area	MAM	79	21	0.22	81	20	–0.62	80	20	–1.47
	JJA	77	18	–0.16	77	18	1.23	79	18	2.66
	SON	46	29	–0.16	45	25	0.68	47	25	0.3
	DJF	42	22	0.31	43	23	0.78	43	22	2.54
Plain area	MAM	55	23	0.44	56	24	0.73	57	22	0.84
	JJA	53	23	–0.09	53	22	0.21	53	22	1.37
	SON	42	26	–0.1	42	23	0.12	43	22	–2.48
	DJF	40	22	0.4	42	18	0.75	43	17	–0.29

During the other two periods (1951–2013 and 1979–2013), MAM and JJA also account for the larger part of the total annual precipitation than SON and DJF (Table 1). The seasonal precipitation has the increasing trends with the largest trend in DJF (0.77 mm/10a) for 1951–2013. For the last three decades (1979–2013), the increasing trend of MAM is equal to those of the other two periods (Table 1). JJA has the largest increasing trend (1.62 mm/10a) which is four times than that of 1951–2013.While a strong decreasing trend (–1.97 mm/10a) is found in SON during 1979–2013. The increasing trend of DJF is the smallest than those of the other periods which is less than one third of that in 1951–2013.

Figure 3 displays the EEMD results of the seasonal precipitation over Central Asia during 1901–2013. For each EEMD component of MAM, it appears a relatively stable quasi-period, with the mean periods of 3 years for c_1, 6 years for c_2, 10 years for c_3, 26 years for c_4 and 54 years for c_5 (Figure 3a and Table 2). c_1 and c_2 display the interannual timescale components of the MAM precipitation with 69% and 20% variance contribution, respectively, indicating that the inter-annual signal is the dominant component of the MAM precipitation over

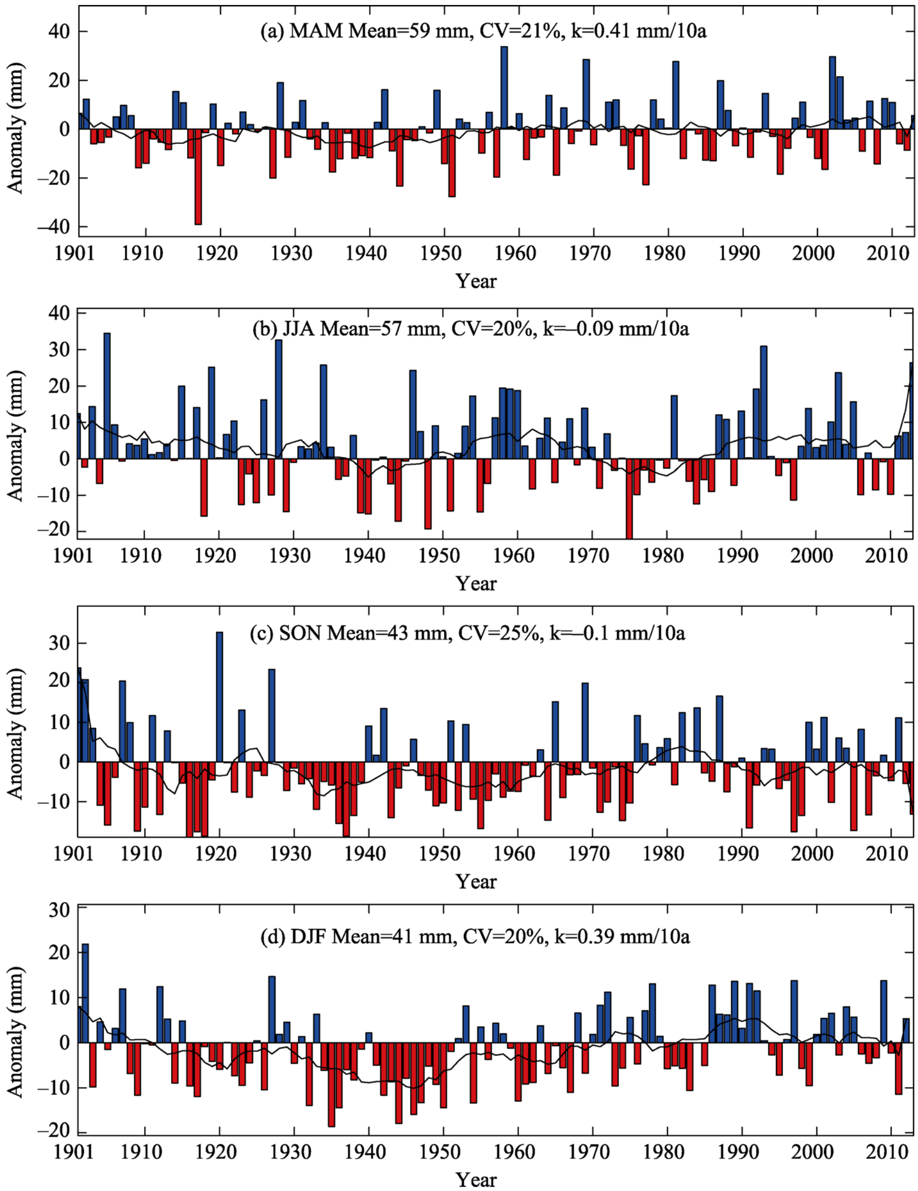

Figure 2 Seasonal precipitation anomalies (a: MAM; b: JJA; c: SON and d: DJF) averaged over Central Asia during 1901–2013, where the reference period is 1961–1990. The thick curve line is the 11-year moving average result.

Central Asia. According to the residual term r, an increasing nonlinear trend with an increment of 8.45 mm is obtained from 1901–2013 which is consistent with the increasing linear trend. For the other seasons, the inter-annual timescale components have 3–6 years mean periods (Figures 3b–3d, Table 2). The inter-annual signal of JJA and SON has 84% and 87% variance contribution, respectively. It is only 59% variance contribution for the variations of the DJF precipitation. Moreover, both JJA and SON have decreasing nonlinear trends based on the residual terms with the values of –3.66 mm and –7.3 mm, respectively (Figures 3b, 3c and Table 2). Contradicting with the increasing linear trend, a decreasing nonlinear trend of

DJF is found with the value of –8.83 mm. During 1951–2013 and 1979–2013, 3–6 years means periods of the seasonal precipitation are also obtained with more than 70% variance contribution which shows that the inter-annual signals are the dominant signal in the variations of the seasonal precipitation (not shown).

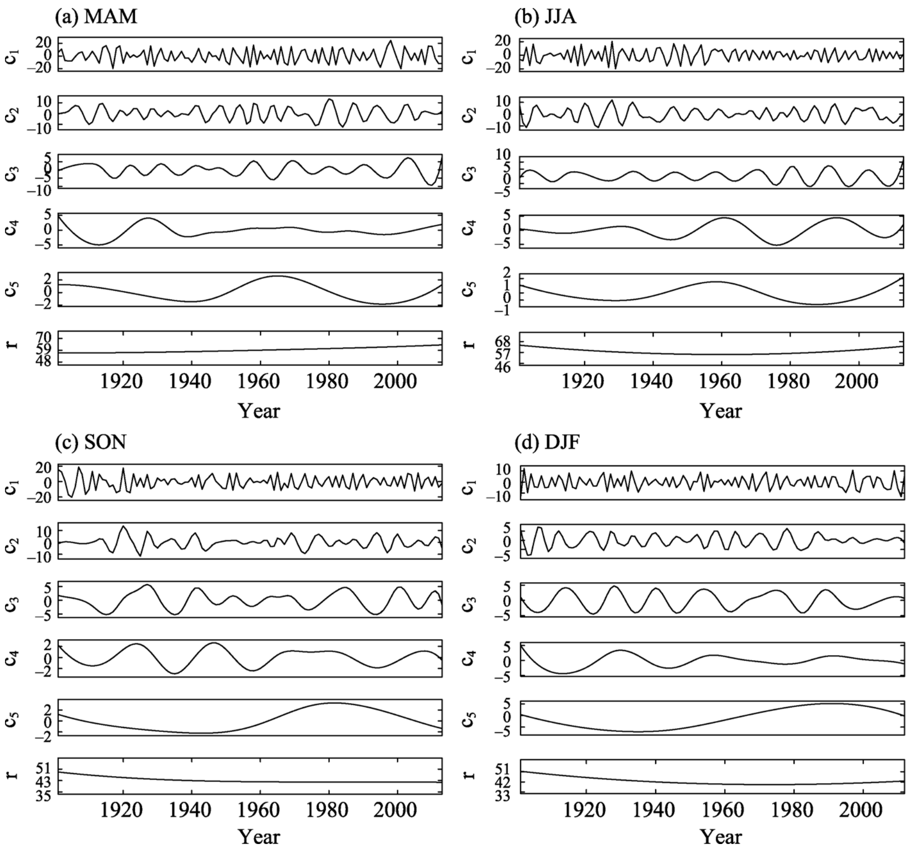

Figure 3 The decomposition results of annual precipitation time series over Central Asia, (a): MAM; (b): JJA; (c): SON and (d): DJF during the period of 1901–2013. The IMF1–IMF5 indicate the different periods of the annual precipitation time series, and the residue term *r* is the nonlinear trend obtained by the EEMD method.

Table 2 Hurst Index (H) of the seasonal precipitation over mountainous area, plain area and Central Asia during 1901–2013, 1951–2013 and 1979–2013

Study area	Season	1901–2013	1951–2013	1979–2013
Central Asia	MAM	0.56	0.62	0.66
	JJA	0.68	0.81	0.75
	SON	0.63	0.76	0.82
	DJF	0.86	0.82	0.92
Mountainous area	MAM	0.58	0.60	0.72
	JJA	0.75	0.86	0.79
	SON	0.55	0.66	0.80
	DJF	0.59	0.74	0.82
Plain area	MAM	0.56	0.63	0.69
	JJA	0.66	0.77	0.73
	SON	0.65	0.78	0.81
	DJF	0.89	0.81	0.98

3.2 Temporal changes over mountainous area and plain area

As the water tower of Central Asia, the mountainous precipitation provides large runoff to the rivers in this region (Chen *et al*., 2012). It also plays an important role on the water resource to the agriculture and animal husbandry of the arid and semiarid ecosystem. In addition, the seasonal variations of the precipitation over mountainous area can result in extreme climate events, such as flood and drought. Therefore, it is necessary to split the entire region into mountainous area and plain area, and then to explore the temporal changes of the seasonal precipitation over the two areas, respectively. In this study, the definition of mountainous area by the United Nations Environment Programme (UNEP) was used; a mountainous area should have elevation >2500 m, or between 1500 m and 2500 m and with a slope >2º, or between 1000 m and 1500 m and with a slope >5º or local elevation >300 m (Blyth *et al*., 2002). Area outside of the mountainous area was treated as plain area.

The mountainous area certainly has the larger mean values of the seasonal precipitation than those of the plain area during the three periods (Table 1). MAM and JJA also have the larger precipitation than SON and DJF over the two separate areas. In 1901–2013, MAM and DJF have the increasing trends both in mountainous area and plain area. It should be noted that the increasing trends of plain area are larger than those of mountainous area, such as 0.44 mm/10a vs 0.22 mm/10a (Table 1). During 1951–2013, except the negative rate of MAM, mountainous area has the positive rates for the other seasons with the largest value in JJA (1.23 mm/10a). In plain area, all the seasonal precipitation has positive trends and DJF has the largest trend (0.75 mm/10a). During the last three decades (1979–2013), in mountainous area MAM has a larger decreasing trend (–1.47 mm/10a) than that of 1951–2013. While the increasing trends of JJA and DJF become larger, such as the DJF with more than three times value from 1979 to 2013 (2.54 mm/10a) than that of 1979–2013 (0.78 mm/10a). Over plain area, the positive trends are found in MAM and JJA, and negative trends appear in SON and DJF.

3.3 Spatial distributions of the linear trends

In this section, the regional differences of the seasonal precipitation are explored by the linear trends of the three different periods (1901–2013, 1951–2013 and 1979–2013) in Figures 4–6. For the MAM precipitation in 1901–2013, more than 60% areas have the increasing trends with the statistically significant at 95% confidence level ($p<0.05$) in 18.87% areas (Table 3). The positive centers mainly occur in northwestern Central Asia and mountainous area, and the decreasing trend centers ($p<0.05$) appear at part of the central Kazakhstan and most parts of Xinjiang (Tarim Basin and Turpan) (Figure 4a). Unlike the spatial distributions of MAM, the increasing trend centers of JJA occur in the mountainous area between Kyrgyzstan and Xinjiang, and small part of northern Kazakhstan (Figure 4b). The areas (such as part of northeast and west of Kazakhstan, northern Xinjiang) with the increasing trend of MAM precipitation become a decreasing trend for the JJA precipitation which result in the equate areas in the liner trends (increasing 50.37% vs decreasing 49.63 in Table 3). Similar spatial distributions are found for SON and DJF (Figures 4c and 4d). Moreover, the increasing trend centers (bigger than 2 mm/10a) of DJF appear in part of northern Kazakhstan and the area between Kazakhstan and Kyrgyzstan which are significant at 95% confidence level

(Figure 4d). Besides the significant decreasing trend in most parts of south and east Xinjiang as MAM, SON and DJF also have the significant decreasing trend in part of the northern Kazakhstan (Figures 4c–4d). Overall, the increasing areas are larger than the decreasing areas for SON and DJF in Table 3.

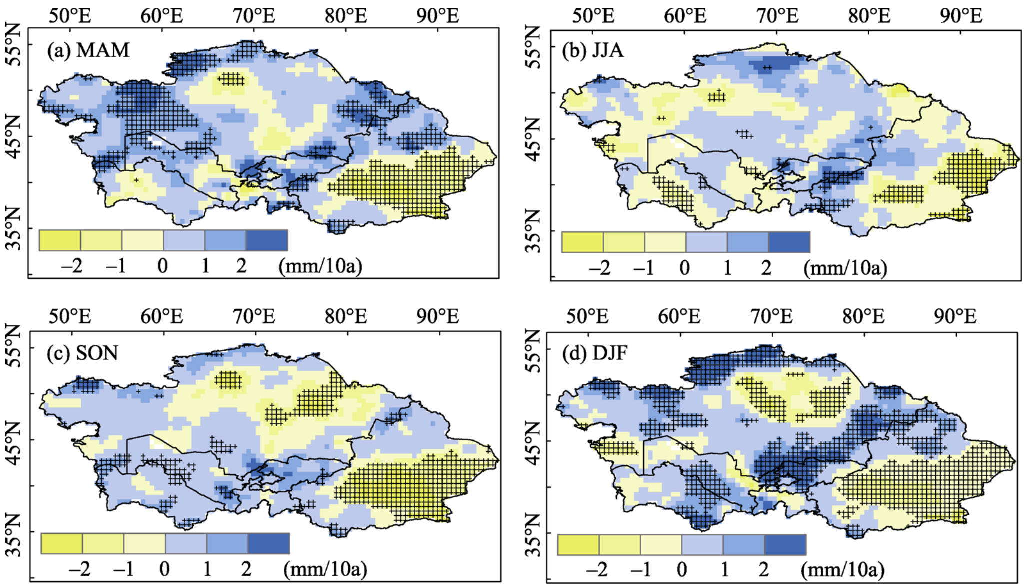

Figure 4 Spatial distributions of the linear trends of the seasonal precipitation over Central Asia during the period of 1901–2013. Statistically significant linear trends at the 95% confidence level are indicated by cross ($p<0.05$).

For 1951–2013, Xinjiang experienced the increasing trend of the four seasons which is contradicted with the decreasing trend during 1901–2013 (Figures 4 and 5). The decreasing trend mainly appears in CAS5 for the other three seasons (e.g. MAM, JJA and SON, Figures

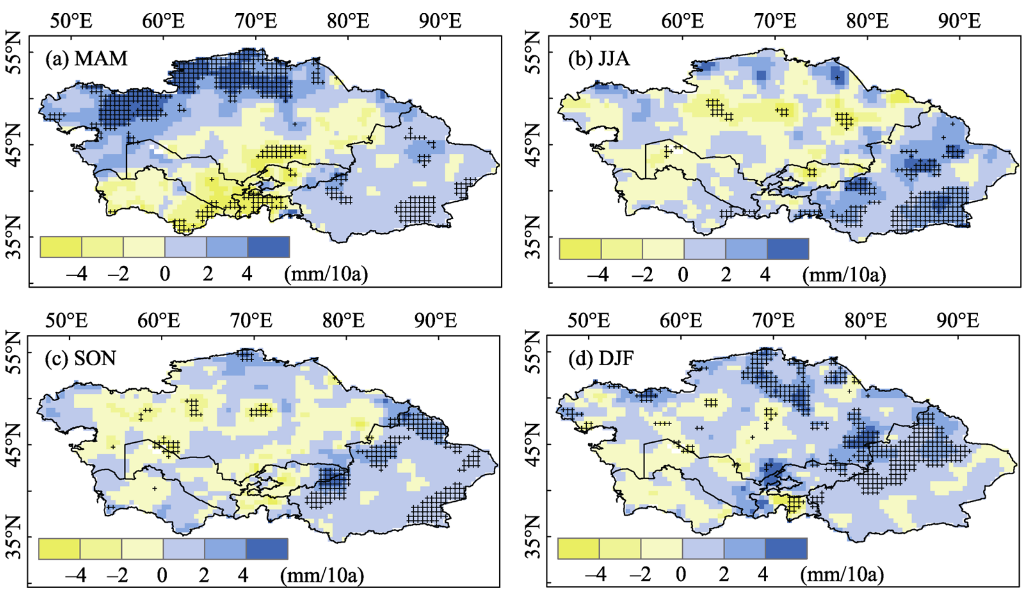

Figure 5 Same as Figure 4, but for the period of 1951–2013

5a–5c) which explain the drying trend in CAS5 and the wetting trend in Xinjiang. Moreover, MAM has the largest significant increasing trend center areas (over the northern Kazakhstan) than those of the other three seasons. The four seasons have the increasing trend areas larger than the decreasing trend areas with the largest increasing trend areas in DJF (71.26%) (Table 3).

For the last three decades, the spatial distributions of the linear trends have large differences among the four seasons (Figure 6). Except SON, the other seasons have the increasing trend areas larger than the decreasing trend areas from Table 3. The increasing trend center (bigger than 4 mm/10a) of MAM is expanded compared with the result in 1951–2013 (Figure 6a). The decreasing trend center still occurs in the middle and south areas of CAS5. The increasing trend center of MAM is shifted to central Kazakhstan and northern Xinjiang at JJA (Figure 6b). For SON and DJF, almost all the CAS5 regions experience a decreased precipitation during 1979–2013 (Figures 6c–6d). The increasing trend centers of DJF appear in mountainous area and northern Xinjiang with the change rate bigger than 4 mm/10a (Figure 6d). It should be noted that considerable parts of Xinjiang have the decreasing trends in the four seasons except DJF.

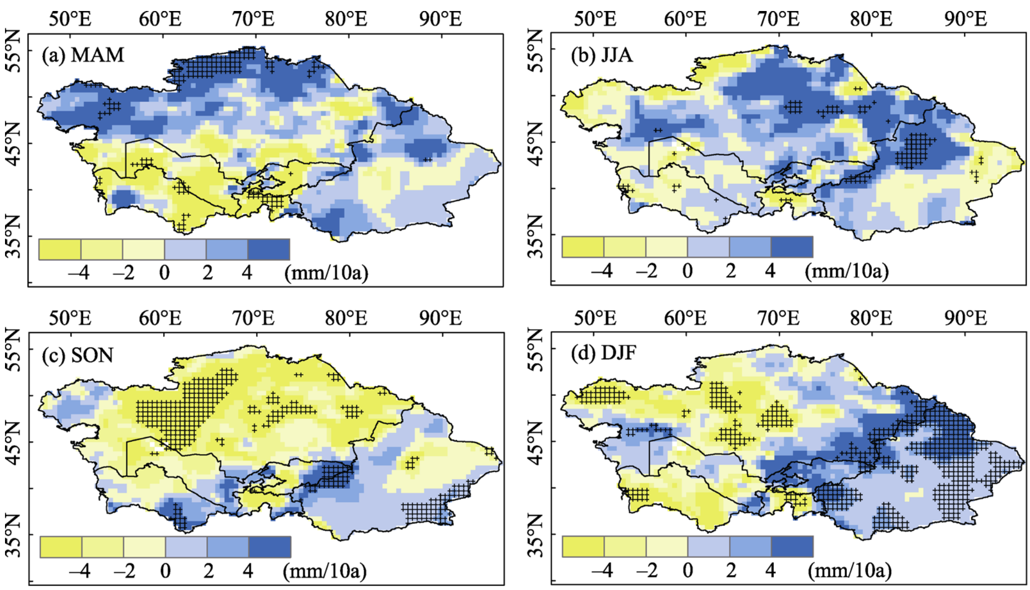

Figure 6 Same as Figure 4, but for the period of 1979–2013

3.4 Leading modes of the inter-annual variations of the seasonal precipitation

In order to further reveal the leading modes of inter-annual variability of the seasonal precipitation over Central Asia, we performed EOF analyses on the seasonal precipitation for the period of 1901–2013. Spatial patterns of the first EOF mode (EOF-1) and the corresponding time coefficients results are shown in Figure 7.

The first EOF mode accounts for 29%, 25%, 27% and 26% of the total variance of MAM, JJA, SON and DJF precipitation, respectively (Figures 7a, 7c, 7e and 7g). Furthermore, these EOF modes are statistically significant at 95% confidence level by the method of North *et al.* (1982). The first EOF modes of MAM and DJF have the similar spatial patterns with the positive values nearly over all Central Asia (Figures 7a and 7g) which indicates that the precipitation have the uniform variations for the two seasons. Moreover, the

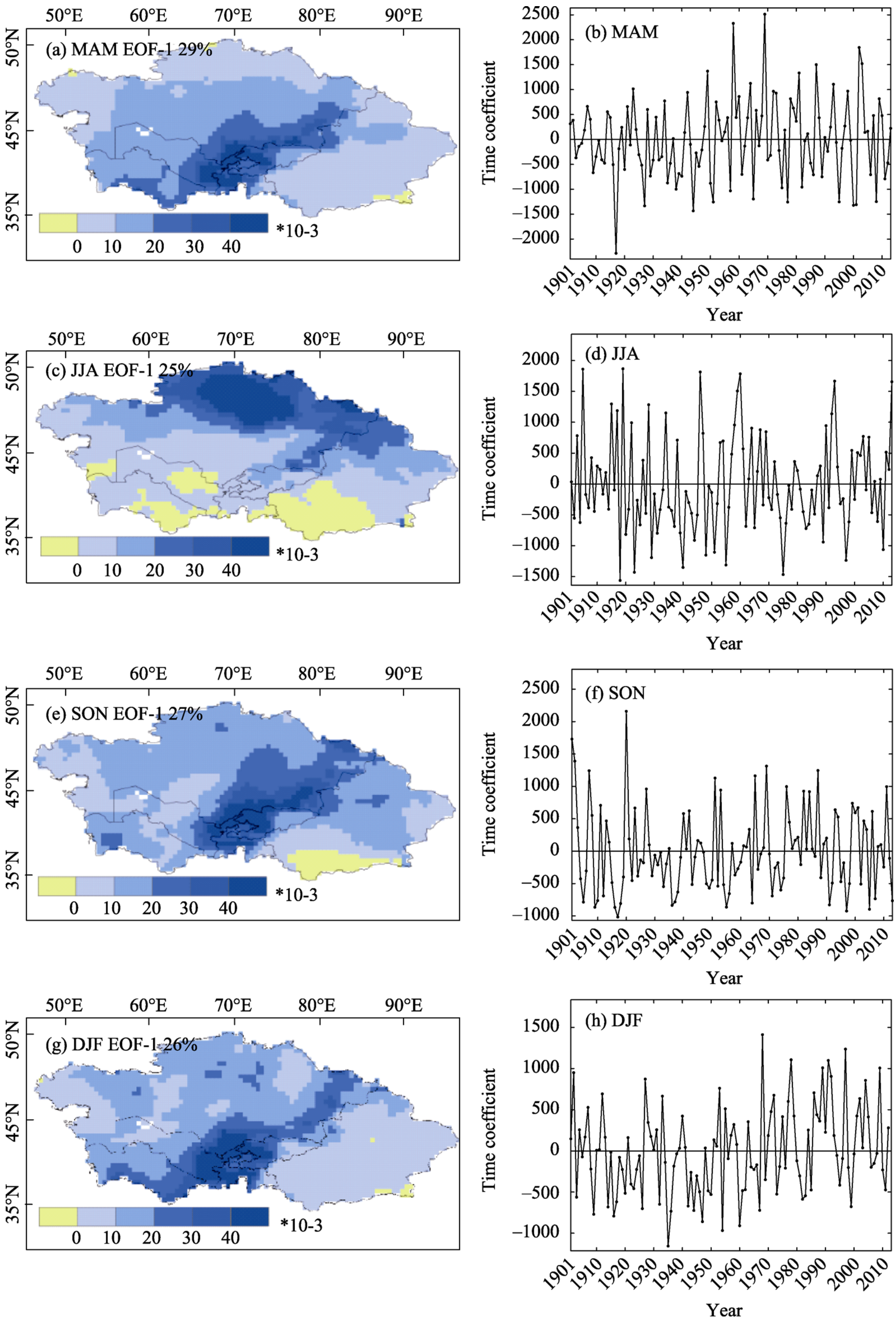

Figure 7 EOF-1 (left panel) of the seasonal precipitation anomalies (mm) and the corresponding time coefficients (right panel) over Central Asia during 1901–2013

positive centers occur in mid-southern Central Asia (such as Kyrgyzstan and Tajikistan), and which shows that these regions have the strongest variations of MAM and DJF precipitation. For JJA, small parts of southwestern Kazakhstan, eastern Uzbekistan, southern Turkmenistan and southwestern Xinjiang have the negative values and the other regions have the positive values which suggest the opposite variations of the precipitation during 1901–2013 (Figure 7c). The positive centers appear in northern Central Asia (e.g. northern Kazakhstan and part of northern Xinjiang). For SON, Figure 7e displays that most regions of Central Asia have positive EOF-1 with the centers occurring in eastern Kazakhstan, Kyrgyzstan and Tajikistan. In general, compared with the other three seasons, JJA has the different variability centers. Figures 7b, 7d, 7f and 7h show the corresponding time coefficients have the similar variabilities as those of the seasonal precipitation in Figure 2. They can capture the wet (dry) years for the seasonal precipitation, such as wet years in 1958, 1969 and 2002 for MAM (Figure 7b) and dry years in 1918, 1923, 1929, 1955 and 1975 for JJA (Figure 7d).

3.5 Relationships between the seasonal precipitation and ENSO

Recent studies (Mariotti, 2007; Hu *et al.*, 2017) suggested that ENSO has strong influences on the magnitude and variability of the precipitation over Central Asia according to the southwesterly water vapor flux coming from the Arabian Sea and tropical Africa. Therefore, in this section, we explore the relationships between the seasonal precipitation and ENSO during 1951–2013. The correlation coefficients and the time lag correlation coefficients will be explored.

With the similar inter-annual variabilities, the seasonal precipitation is significantly positively correlated with the ENSO at MAM (CC=0.35, p<0.01), SON (CC=0.27, p<0.05) and DJF (CC=0.5, p<0.01) during 1951–2013 (Figure 8 and Table 4), respectively. It indicates that ENSO has the largest impact on the precipitation in winter, followed by spring. For JJA, the correlation value is only 0.03 which shows that there is no (or slightly) correlation between the precipitation and ENSO. ENSO has the positive impacts on the seasonal precipitation

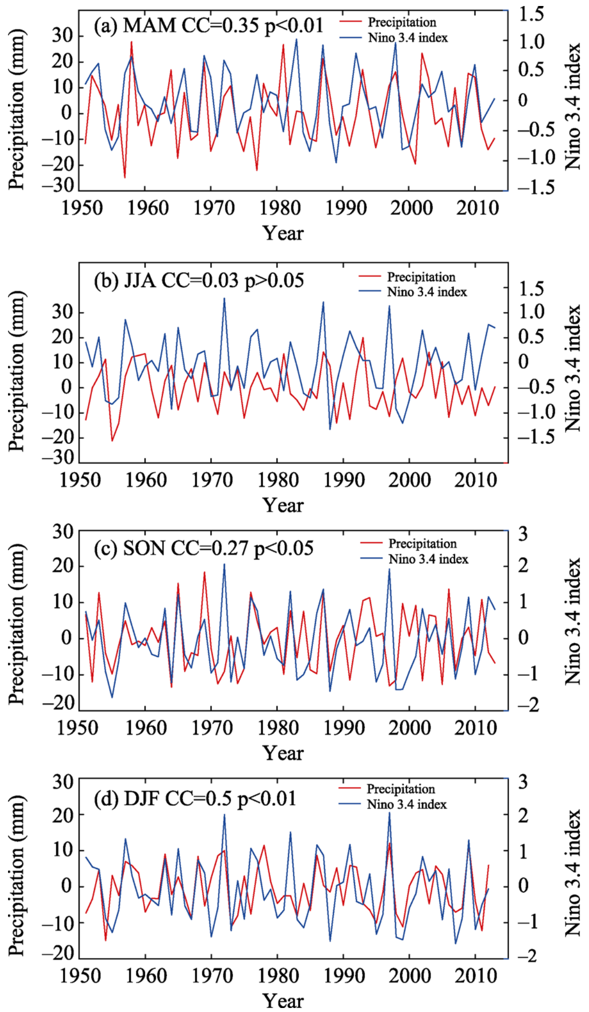

Figure 8 Inter-annual signals of the seasonal precipitation and Niño 3.4 index obtained by EEMD method during 1951–2013

at MAM and DJF with significant correlations ($p<0.05$), especially after 1970s (Figure 9a), while the precipitation of JJA and SON has no significant correlation with ENSO except the CC in 1951 for SON. In order to further reveal the correlations between the seasonal precipitation and ENSO, the 30-yr moving CC values are computed in Figure 9b. The results show that the positive correlation coefficients of MAM and DJF increase with time, while it is decreasing for JJA and SON. Moreover, almost of the 30-yr moving CC values of DJF are significant at 95% confidence level, and for MAM the CC values are only significant after 1978 for ($p<0.05$). It is interesting that the positive CC values of SON are the largest than those of MAM and DJF for the starting years of 30-yr moving CC from 1951 to 1965 (Figure 9b). Obviously, these CC values of SON are significant at 95% confidence level. This can be well explained by the temporal variabilities of the seasonal precipitation and ENSO (Figures 8a, 8c and 8d). In general, from the above analyses, it can be concluded that the strongly positive correlations identified between the precipitation and ENSO in DJF are stable (or robust) in time.

Table 3 Percentage areas (%) with the increasing trend, decreasing trend, significant increasing trend (SIT) and significant decreasing trend (SDT) at 95% confidence level of the four seasonal precipitation during 1901–2013, 1951–2013 and 1979–2013

Period	Season	Increase	Decrease	SI	SD
1901–2013	MAM	69.00	31.00	18.78	11.83
	JJA	50.37	49.63	3.01	9.06
	SON	57.40	42.60	6.60	16.48
	DJF	60.99	39.01	26.67	20.34
1951–2013	MAM	66.50	33.50	17.22	3.71
	JJA	57.75	42.25	9.25	1.72
	SON	60.95	39.05	9.57	1.87
	DJF	71.26	28.74	16.56	1.95
1979–2013	MAM	61.07	38.93	4.22	1.87
	JJA	63.30	36.70	3.44	0.86
	SON	32.57	67.43	4.49	10.39
	DJF	58.53	41.47	17.77	6.21

Moreover, we further explore the lag season relationships between the precipitation and Niño 3.4 index during 1951–2013 in Table 4. The lag-i (i=0, 1, 2, 3, 4) is computed to reveal the effects of ENSO on the precipitation. Taking the CC values of MAM in the first row as an example, lag-0 CC is obtained between the MAM precipitation and MAM Niño 3.4 index at the same year during the period of 1950–2013. The lag-1, lag-2, and lag-3 CC of MAM is computed between the MAM precipitation and the JJA, SON and DJF Niño 3.4 index at the same year, respectively. The last value lag-4 CC of MAM is obtained between the MAM precipitation and the next year MAM Niño 3.4 index. The lag-i (i=0, 1, 2, 3, 4) values of the other seasons are obtained by the same approach. The results in Table 4 show that the significant influences of ENSO are persistent till the JJA precipitation with CC=0.31. Although there is no relationship between the JJA precipitation and JJA Niño 3.4 index, ENSO has the great influences on the SON and DJF precipitation of the same year, and the MAM and JJA precipitation of the next year with the significant positive CC values in Table 4. ENSO has significant positive impact on the SON (CC=0.27) and DJF (CC=0.47) precipitation in the present year and this influence will last until the JJA precipitation in the next year. The significantly positive effects of ENSO on the precipitation are from DJF in the same year to JJA in the next year from the lag CC values in Table 4. These results indicate that the time lags are obtained between the seasonal precipitation and ENSO.

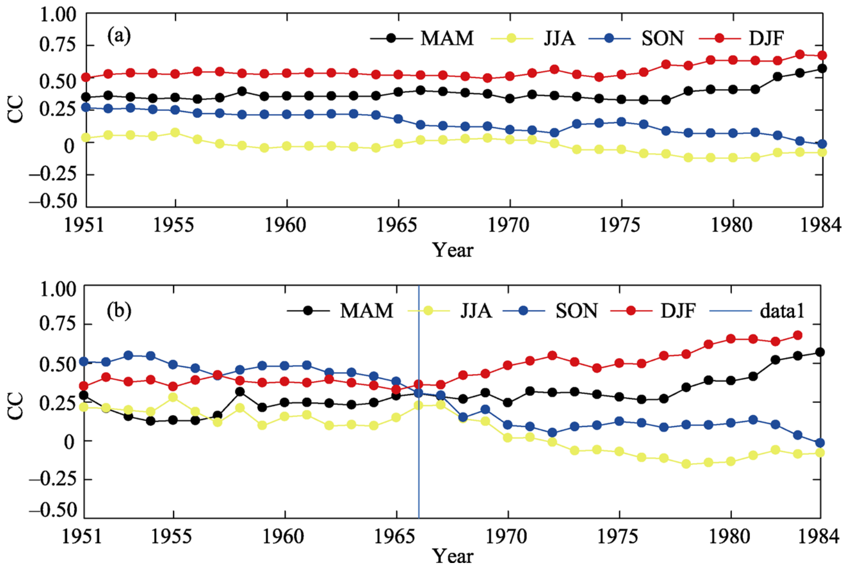

Figure 9 CC results of the inter-annual signals between seasonal precipitation and Niño 3.4 index during 1951–2013, (a) CC of the periods from year *i* to 2013 (i = 1951, …, 1984) and (b) 30-yr moving CC, where the vertical blue line is in the year 1966

Table 4 CC results of the seasonal lags time series between the precipitation and Niño 3.4 index during 1951–2013, lag-i (i=0, 1, 2, 3, 4) means lag i seasons

Seasonal lag	MAM	JJA	SON	DJF
lag-0	0.35*	0.03	0.27*	0.5**
lag-1	0.31*	0.27*	0.47**	0.42**
lag-2	0.12	0.44**	0.38**	0.32*
lag-3	0.11	0.44**	0.32*	–0.12
lag-4	0.22	0.36**	–0.21	0.11

In order to display the spatial relationships between the seasonal precipitation and ENSO, the spatial patterns of the seasonal correlation coefficient results are provided in Figure 10. In this paper, we should note that we only provide the spatial patterns of lag-0 CC results for each season and the other lag CC patterns are not considered. For MAM, except the parts of northwestern Kazakhstan, the CC values are positive in Central Asia during 1951–2013 (Figure 10a). More than 30% regions have the significant CC values which mainly occur in eastern Kazakhstan, Kyrgyzstan, Tajikistan and most parts of Xinjiang (such as Junggar Basin, Turfan Depression and southeastern Xinjiang). Figure 10b shows that the CC values are disorderly distributed over the entire region with positive or negative values for JJA, and the area with significant values is less than 5%. From Figure 10c, most areas of Central Asia (71%) have positive correlations between the SON precipitation and ENSO, and the areas (12%) with significantly positive values mainly appear in eastern and southern CAS5. The negative values occur in parts of western Kazakhstan, Turfan Depression and Tarim Basin. For DJF, except the negative values in southwestern Xinjiang, more than 92% regions have the positive values and the significant regions mainly appeared over CAS5 (Figure 10d).

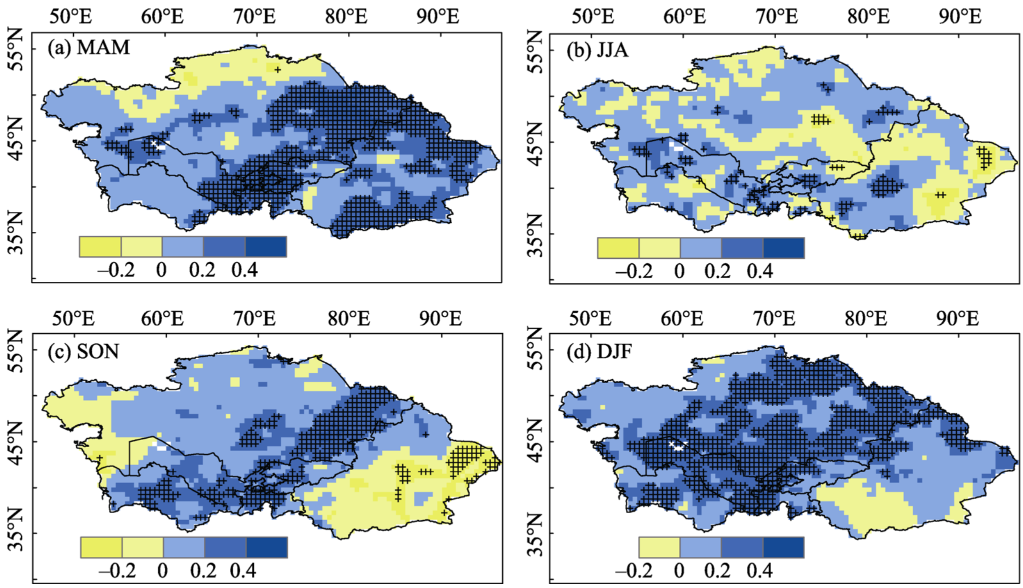

Figure 10 Spatial distributions of the correlation coefficients of the inter-annual signals between the seasonal precipitation and Niño 3.4 during 1951–2013, where the cross symbols are the correlation coefficient values significantly at 95% confidence level

In summary, ENSO has significantly positive impact on the precipitation in MAM, SON and DJF during 1951–2013, although the impact on SON becomes weak after 1966. However, the influence of ENSO on JJA precipitation is weak. In addition, the main affected regions by ENSO are different for the three seasons which suggests that the precipitation of MAM, SON and DJF may be controlled by different atmospheric circulations during ENSO events. Therefore, the possible physical mechanisms associated with the seasonal precipitation should be discussed from the perspective of ENSO events.

3.6 Composite analysis based on ENSO events

Composite analyses of precipitation and water vapor flux fields using El Niño minus La Niña years (Table 5) are conducted to discuss the possible physical processes during 1951–2013. Because of the weak influence of ENSO on the JJA precipitation, in this section, we only consider MAM, SON and DJF. During El Niño, there are more precipitation than the normal ENSO and La Niña over most parts of Central Asia, especially the middle southern region (Figure 11). For MAM, most of the areas with the positive anomalies are significant at 95% confidence level (Figure 11a). While only few areas have significant differences for SON and DJF (Figures 11b and 11c) which may be caused by their little precipitation. Furthermore, the composite differences of the three seasons have similar spatial distributions as the correlation coefficients between the seasonal precipitation and Niño 3.4 (Figures 10 and 11).

Table 5 El Niño and La Niña years used in the composite analyses

Season	El Niño	La Niña
MAM	1958, 1969, 1983, 1987, 1992, 1993, 1998, 2005, 2010	1955, 1956, 1967, 1968, 1971, 1974, 1975, 1985, 1989, 1999, 2000, 2008
JJA	1957, 1965, 1972, 1982, 1987, 1991, 1992, 1997, 2002, 2004, 2009	1954, 1955, 1956, 1964, 1970, 1973, 1974, 1975, 1988, 1999, 2010
SON	1965, 1972, 1982, 1987, 1991, 2002, 2004, 2006, 2009	1954, 1955, 1964, 1970, 1973, 1975, 1988, 1998, 1999, 2010
DJF	1957, 1965, 1972, 1982, 1986, 1991, 1994, 1997, 2002, 2009	1955, 1970, 1973, 1975, 1988, 1998, 1999, 2007, 2010

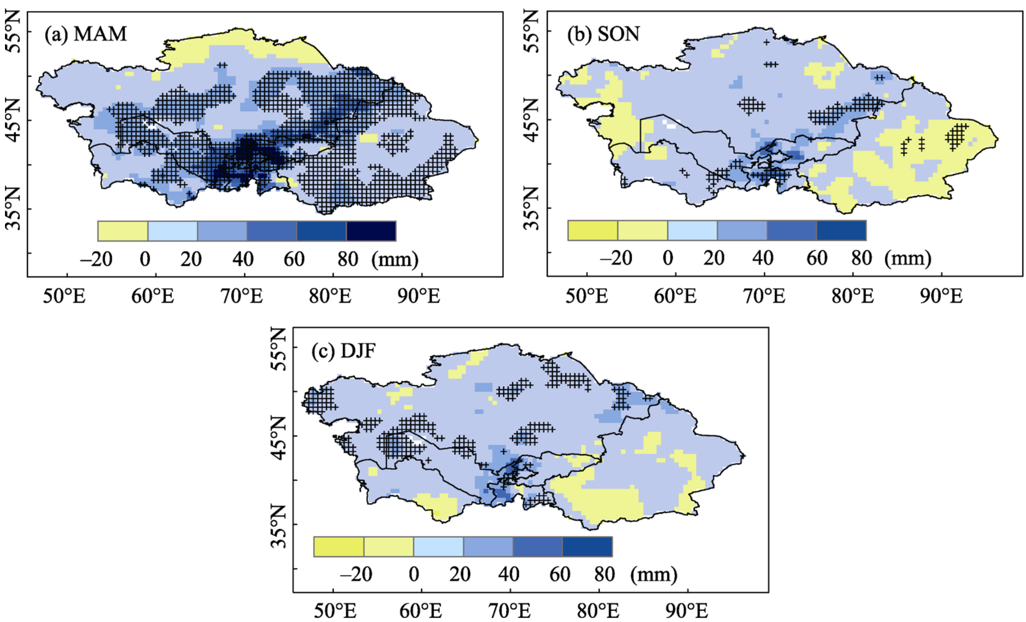

Figure 11 The El Niño minus La Niña composite difference in seasonal precipitation: (a) MAM, (b) SON and (c) DJF during 1951–2013, where the cross symbols are the different values significantly at 95% confidence level

From the composite result of the water vapor flux, southwesterly water vapor fluxes generated in Indian and western Pacific Oceans enhanced the MAM precipitation over middle and south Central Asia during warm ENSO events (Figure 12a). Particularly, the above water vapor fluxes have the following major paths: Saudi Arabia (sourced in Indian Ocean)→Iraq→Iran→Central Asia and the Mediterranean Sea (sourced in western Atlantic Ocean)→Libya→Iraq→Iran→Central Asia. In addition, a northeastern water vapor flux from Russia (sourced in the Arctic Ocean) increased the MAM precipitation over north Central Asia. For the SON precipitation, the southwesterly flux brings moisture to middle and south Central Asia across the Arabian Peninsula (Figure 12a). Compared with the water vapor flux of MAM and SON, there are two major water vapor flux transport paths for the DJF precipitation: one path (generated in Indian and western Pacific Oceans) is the Arabic Sea→India→Pakistan→Afghanistan→Central Asia; the other path is the Mediterranean Sea→Turkey→the Black Sea→Central Asia (Figure 12c). It should be noted that MAM has more water vapor fluxes than SON and DJF which is agreed with the more precipitation in MAM over Central Asia. Moreover, the north water vapor fluxes are only detected in MAM. Overall, the above analyses suggest that the southwesterly water vapor flux from the Arabic Sea and Africa is the source of Central Asia precipitation during El Niño. Among the seasons, MAM has the largest precipitation which is associated with the largest water vapor flux. Furthermore, these water vapor fluxes are mainly generated in Indian and western Pacific Oceans. These results are consistent with previous studies by Mariotti (2007) and Hu *et al*. (2017).

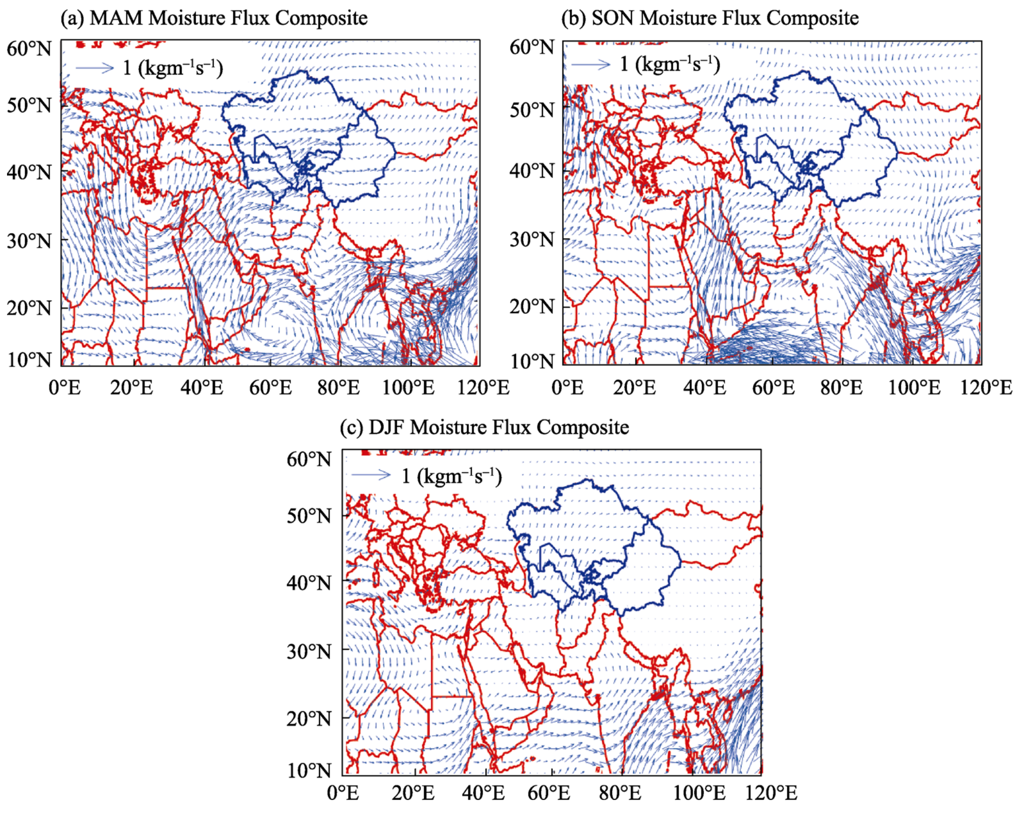

Figure 12 The El Niño minus La Niña composite difference in moisture flux: (a) MAM, (b) SON and (c) DJF during 1951–2010

The corresponding seasonal divergence of the total moisture fluxes (only including the region: 30°–120°E and 30°–90°N) are displayed in Figure 13. The MAM divergences of the total moisture fluxes have the negative anomalies across most areas of Central Asia with the center in the middle southern regions (Figure 13a) which indicate the water vapor convergence and result in the more precipitation in El Niño years than La Niña years (Figure 11a). Furthermore, the negative anomaly center of the MAM moisture divergences over the middle southern regions is statistically significant at 95% confidence level ($p<0.05$). For the other two seasons (SON and DJF in Figures 13b and 13c), the negative anomalies mostly occur over CAS5 and the positive anomalies appear in large areas of Xinjiang which superimpose with the total moisture flux anomalies to illustrate the spatial patterns of the precipitation in Figures 11b and 11c.

3.7 Atmospheric circulation response to ENSO

Comparing with La Niña, most of the low-latitude region south of 40°N is dominated by significantly anomalous high pressure when El Niño occurs in spring. North of this abnormal high pressure, there is a weak low pressure anomaly center across Eastern Europe to the western part of Central Asia, with a deeper trough around the Mediterranean Sea and a high pressure ridge in Middle East region (Figure 14a). Such atmospheric circulation pattern enhances the westerly (Figure 14b) and thus is favorable for transporting lager amount of water vapor from the Mediterranean Sea and Indian Ocean to Central Asia (Wang *et al*., 2014; Huang *et al*., 2015). That is the southwestern and western water vapor path for Central Asia reinforces during El Niño. In addition, another significant high pressure centre exists over Barents Sea and cooperates with the anomalous low pressure center, and then results in enhanced northeastlies and cold moisture from Arctic Ocean (northern moisture path). The similar pattern is also found in the upper troposphere (Figures 14a and 14b). The cold and warm moisture air flow meet around Central Asia and thereby causes a rainy spring during El Niño.

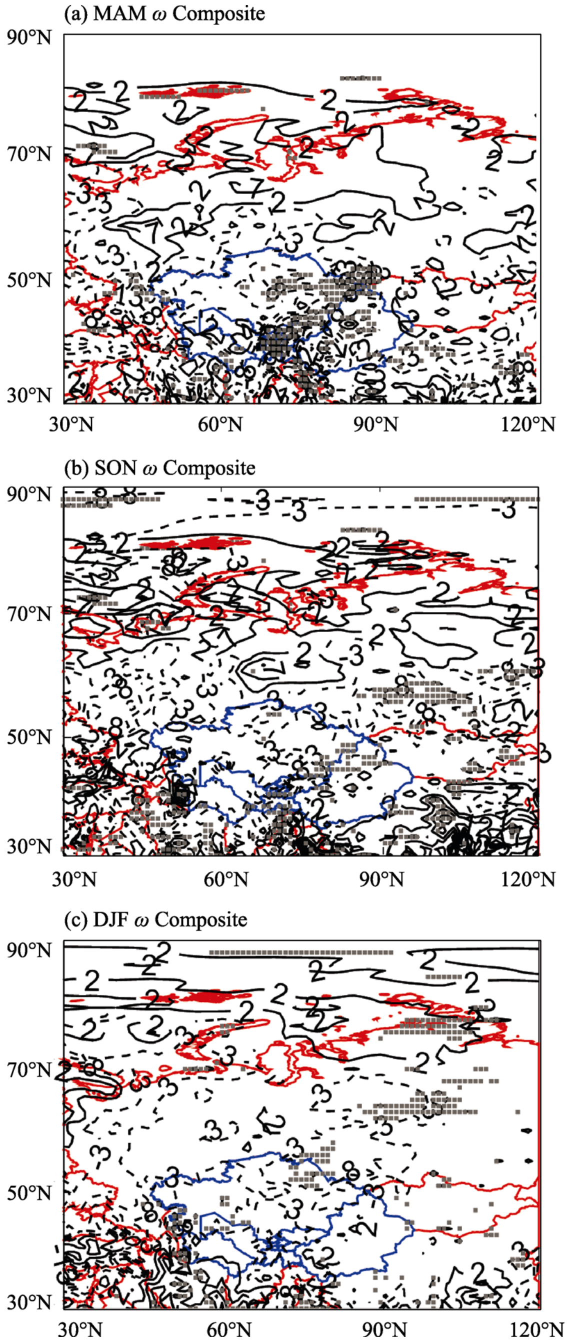

Figure 13 ENSO-based composites of divergences of the total moisture fluxes for MAM, SON and DJF during 1950–2013. The contour interval is 5×10^{-6} kg/m^2/s and the gray areas denote regions significant at the 95% level (p<0.05) by the student's t-test. The zero contour is omitted and dashed lines are negative.

In autumn, vast range of positive anomalies in geopotential height still appears south of 40°N when El Niño occurs, and thereby strengthening the warm and moist southwesterly to Central Asia and thus more precipitation. While there is no negative pressure anomalies over Central Asia and at the same time an abnormal high pressure dominates the whole region of Eurasia mid-high latitude, with an anomalous anticyclonic ridge in the lower troposphere around Central Asia (Figure 14c). In front of such anticyclonic ridge, anomalous northeasterly meets with moist southwesterly and thereby enhancing the convergence and upward motion in eastern and southern CAS5 (Figure 14d), which explains well

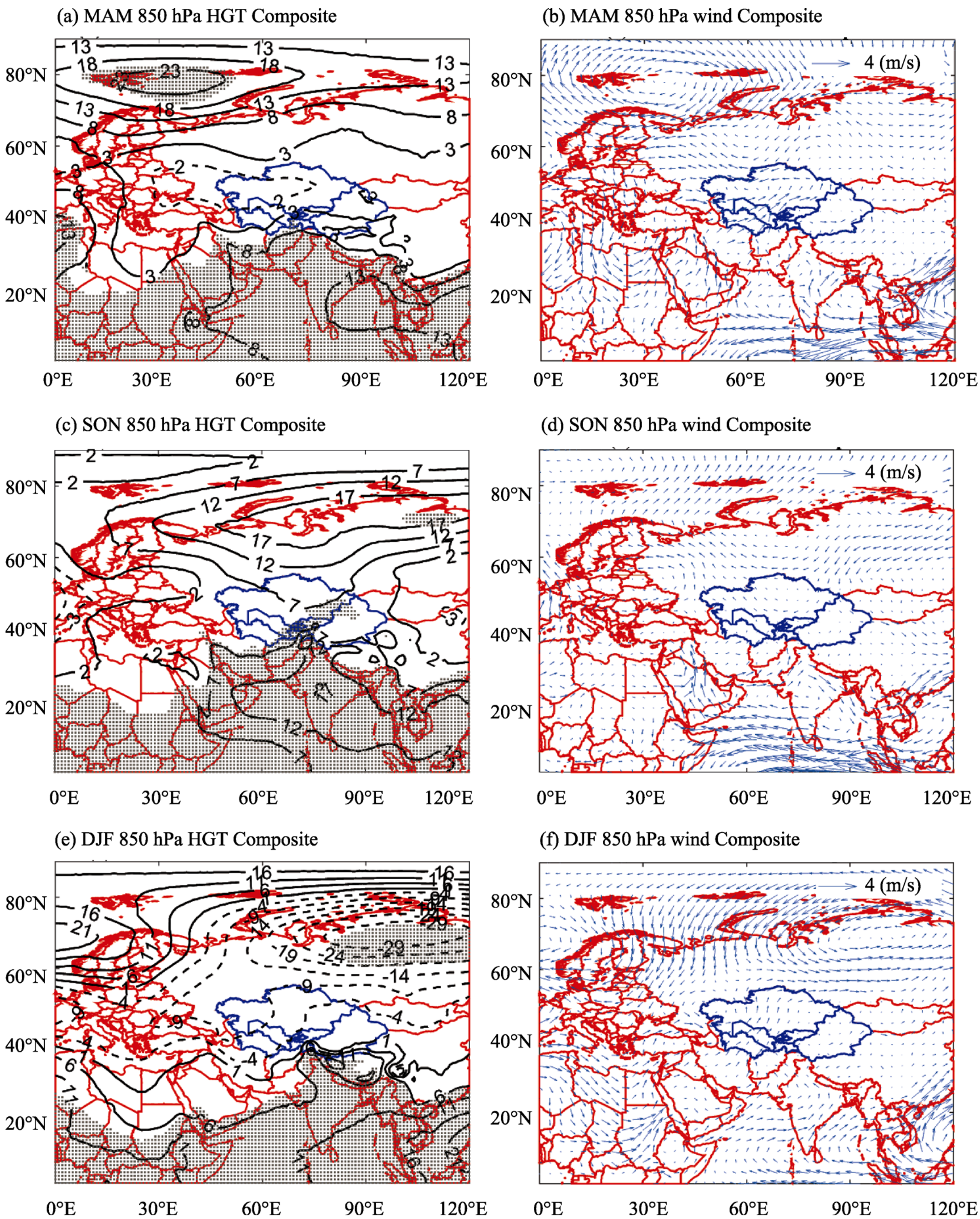

Figure 14 ENSO-based composites of geopotential height (HGT) (left column) and wind for MAM, SON and DJF at 850 hPa during 1950–2013. The contour interval is 5 m for HGT and the gray areas denote regions significant at the 95% level (p<0.05) by the student's t-test. The zero contour is omitted and dashed lines are negative.

the abundant precipitation particularly in these regions during El Niño autumn. In the upper troposphere, there is an obvious tripole structure in the meridional direction, and Central Asia is between the anomalous high- and low-pressure center (Figure 15c) and thus experiences a weakened westerly jet (Figure 15d). It implies the western water vapor path fails in autumn when El Niño occurs, which explains to some extent why the El Niño-induced precipitation in autumn is less than that in spring.

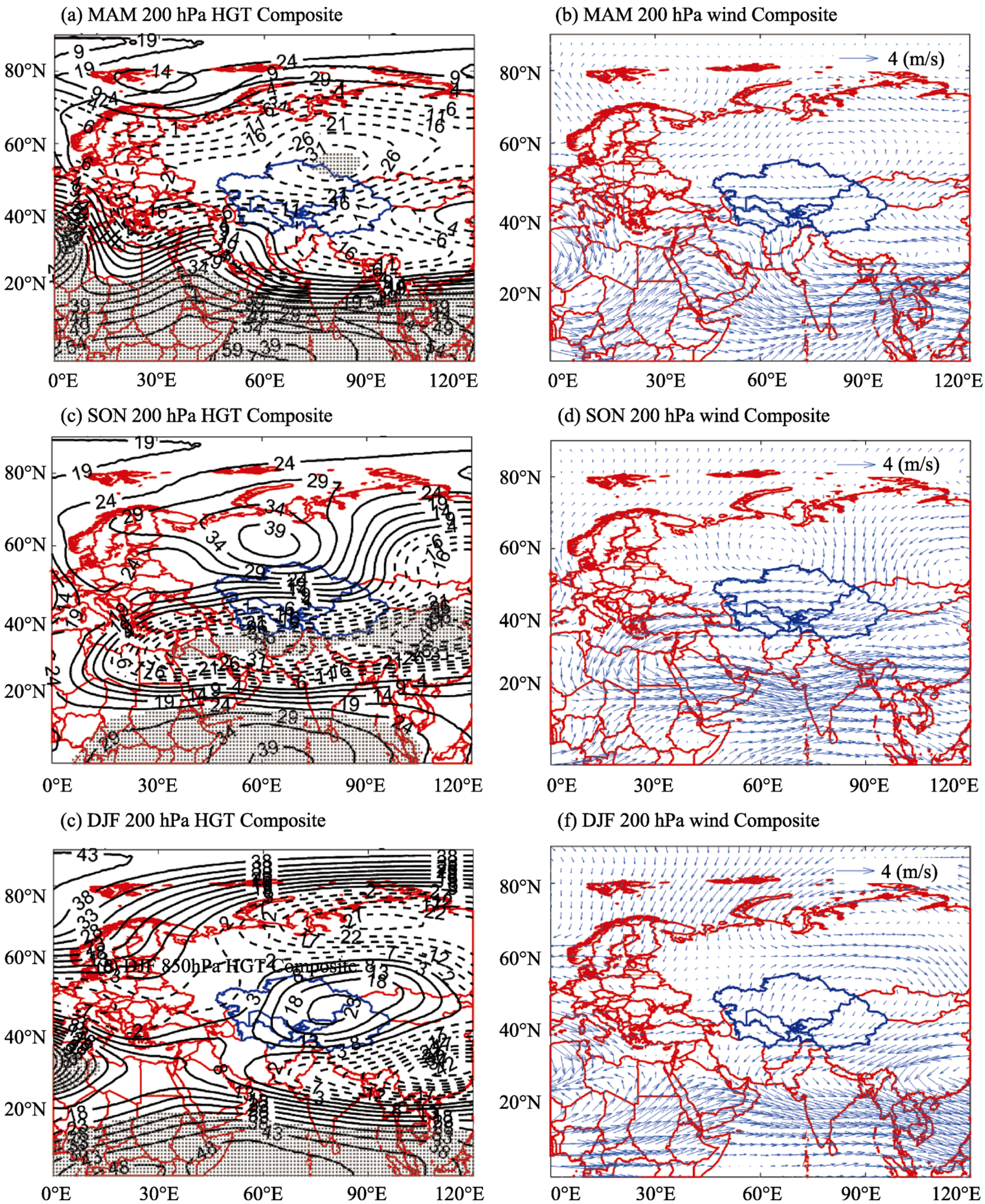

Figure 15 Same as Figure 14 but for 200 hPa

As for wintertime, the southeastern water vapor path sourced in Indian Ocean is stronger because of the significantly positive geopotential height in the low latitudes. Meanwhile, most of middle-high latitudes is under the control of abnormal low pressure, with the center around the Siberia (Figures 14e and 14f). Above atmospheric circulation pattern also results in a much stronger westerly and thus strengthens the western water vapor path for Central Asia (Wang *et al*., 2014). At the same time, the anomalous high pressure center in upper troposphere cooperates with the anomalous low pressure center in lower troposphere over Central Asia (Figures 15e and 15f), which promote the water vapor convergence upward movement and causes the winter more precipitation in these regions.

4 Discussion

4.1 Comparison of this study with prior studies

Our results show that the precipitation experienced increasing trend in MAM and DJF over Central Asia during 1901–2013, which is consistent with the rising trend at the same seasons in Pacific Northwest of the United States (Abatzoglou *et al*., 2014, Table 6). In consistent with the increased seasonal precipitation over mid to high latitudes of Northern Hemisphere during the past half century (Sarojini *et al*., 2012; Noake *et al*., 2012), Central Asia has the increasing trends at seasonal scales during 1951–2013 (Table 6). Of which, the predominantly increased areas occurred in Xinjiang, which is obtained by recent studies based on the precipitation recording from stations (Wang and Yan, 2010; Li *et al*., 2011). But it is decreased for the seasonal precipitation over Iberian Peninsula (De Luis *et al*., 2009; De Luis *et al*., 2010) during 1946–2005 and 1951–2000. For the period of 1979–2013, JJA precipitation has increasing trend over Central Asia and this increasing trend of JJA is also detected over southeastern and northwestern China during 1978–2002 (Yao *et al*., 2008). Furthermore, among the four seasons MAM and DJF have the largest trends during the three periods.

As for the ENSO-related precipitation in other regions, ENSO also has large impacts on the variations of the seasonal precipitation over Central Asia. Specially, precipitation in MAM, SON and DJF over Central Asia are significantly positively correlated with ENSO which agree with the results obtained in southwest Central Asia (Mariotti, 2007), southwest Asia (Hoell *et al*., 2012, 2015, 2017), Yangtze River basin, China (Xiao *et al*., 2015) and northwestern China (Li *et al*., 2016). In Europe, significant ENSO-associated changes in precipitation are evident during the boreal spring and fall seasons, marginal during boreal summer, and absent during boreal winter (Shaman, 2014). The strong links between ENSO and MAM precipitation also existed in the region 47.5°–52.5°N, 35°E–5°W of Europe from 1851 to 1993 (Van Oldenborgh *et al*., 2000). During summer and fall increased precipitation over southern Europe occurs when El Niño conditions prevail in the equatorial Pacific (Park, 2004). It has been found that wintertime precipitation increased over Britain, France, and Germany during the El Niño events, but precipitation decreased over Scandinavia (Zanchettin *et al*., 2008).

These ENSO teleconnections to seasonal precipitation can provide an approach to predict the precipitation at regional and global scales (Van Oldenborgh *et al*., 2000; Chiodi and Harrison 2015), and obviously can be applied to the seasonal precipitation over Central Asia.

Table 6 Comparison of decadal seasonal precipitation change rate (mm/10a or %/10a) of Central Asia from 1901 to 2013 from this study to rates reported in other studies, where + means increasing trend, – means decreasing trend, CMIP5 (Coupled Model Intercomparison Project, phase 5), MOPREDAS (Monthly Precipitation Database of Spain), USHCN v2.5 (U.S. Historical Climate Network, version 2.5), Climatic Research Unit (CRU) TS3.21 dataset, NH (Northern Hemispheres)

Studies	Study area	Study period	Data	MAM	JJA	SON	DJF
Abatzoglou *et al*. (2014)	Pacific Northwest of the United States	1901–2012	USHCN v2.5, PRISM, CRU TS3.21 and U.S. climate division dataset	1.8%/10a	1.3%/10a	0	0.2%/10a
Noake *et al*. (2012)	Globe	1952–1999	VASClimO, Zhang, CRU and CMIP3	+mid to high latitude of NH	+ mid to high latitude of NH	+ mid to high latitude of NH	+mid to high latitude of NH
Sarojini *et al*. (2012)	Globe	1951–2005	Zhang and CMIP5	+ high latitude of NH	+ high latitude of NH	+ high latitude of NH	+ high latitude of NH
Yao *et al*. (2008)	Asia	1978–2002	Gridded dataset from Xie *et al*. (2007)		+ southeastern and northwestern China		
Wang and Yan (2009)	China	1961–2007	587 stations	+ northwestern China	+ northwestern China	+ northwestern China	+ north-western China
De Luis *et al*. (2010)	Iberian Peninsula	1946–2005	MOPREDA	–		+	–
De Luis *et al*. (2009)	Mediter-ranean Iberian Peninsula	1951–2000	MOPREDA	–5.5 mm/10a	–4.4 mm/10a	–1.8 mm/10a	–2.2 mm/10a
Li *et al*.(2011)	Xinjiang	1961–2005	65 stations	–1.08 mm/10a	1.8 mm/10a		2.1 mm/10a
Our study	Central Asia	1901–2013	GPCC V7	0.41 mm/10a	–0.09 mm/10a	–0.1 mm/10a	0.39 mm/10a
		1951–2013		0.49 mm/10a	0.4 mm/10a	0.23 mm/10a	0.77 mm/10a
		1979–2013		0.42 mm/10a	1.62 mm/10a	–1.97 mm/10a	0.24 mm/10a

Moreover, according to the composite analyses of our results, Mariotti (2007) suggested that enhanced precipitation in southwest Central Asia during warm ENSO events results from an anomalous southwesterly water vapor flux across the Arabian Peninsula coming from the Arabian Sea and tropical Africa, which is generated along the northwestern flank of the high pressure anomaly over the Indian and western Pacific Oceans, part of the ENSO see pressure anomalies.

Furthermore, the lagged associations between the seasonal ENSO and seasonal precipitation are detected over Central Asia, especially the persistent influences of ENSO in SON and DJF on the following JJA precipitation. Although the ENSO signals in JJA have little influence on the synchronous precipitation over Central Asia, it has significant positive lag-impact on the September-August precipitation in these regions (Table 4). Evidence for lagged correlations between Northern Hemisphere wintertime ENSO conditions and precipitation the following spring has also observed in many other regions, including southwestern Europe (Knippertz *et al*., 2003), central Europe (Lloyd-Hughes and Saunders, 2002), and Scandinavia (Feddersen, 2003). These lag associations may be caused by the seasonal persistence of SST anomalies in the tropical Pacific (Shaman, 2014).

4.2 Relationships between the seasonal precipitation, temperature and NDVI

It is known that there exist strong relationships between precipitation and temperature at global and regional scales (e.g. Madden and Williams, 1978; Zhao and Khalil, 1993; Trenberth and Shea, 2005; Berg *et al*., 2009) due to the close links between the air's moisture-holding capacity and the temperature. Over land, negative correlations dominate because the dry conditions favor more sunshine and less evaporative cooling, while wet summers are cool. Positive correlations dominate over high latitudes in winter because warm moist advection in extratropical cyclones favors precipitation and the water holding capacity of the atmosphere limits precipitation amounts in cold conditions (Trenberth and Shea, 2005).

For Central Asia, increasing trend of the surface temperature has been detected in the 20th century, especially for MAM during 1979–2013 (Hu *et al*., 2014). In this section, we explore the relationship between the seasonal precipitation and temperature. The temperature is from the global monthly CRU TS 3.24 dataset with the spatial resolution of 0.5°×0.5° during 1901–2015 (https://crudata.uea.ac.uk/cru/data/hrg/cru_ts_3.24/). Negative correlations are obtained between the precipitation and temperature in MAM and JJA during the three periods (Table 7), especially for JJA (CC=–0.24) during 1901–2013 which is consistent with the dry conditions following more sunshine and wet summers being cool (Trenberth and Shea 2005). The SON precipitation is positively correlated with the temperature during 1901–2013 and 1951–2013, and it is a negative correlation for 1979–2013. In DJF, the precipitation is positively correlated with the temperature for the three periods, and which is caused by the warm moist advection in extratropical cyclones favors precipitation and the water holding capacity of the atmosphere limits precipitation amounts in cold conditions (Trenberth and Shea, 2005).

Moreover, we detect the relationships between the seasonal precipitation and the normalized difference vegetation index (NDVI) over Central Asia during 1982–2012. The NDVI data with a spatial resolution of 8 km × 8 km and 15-day interval are downloaded from the Global Inventory Monitoring and Modeling Studies (GIMMS) group derived from the advanced very high-resolution radiometer (AVHRR) of the National Oceanic and Atmospheric Administration (NOAA) Land dataset for the period January 1982 to December 2012 (ftp://ftp.glcf.umiacs.umd.edu/glcf/GIMMS/, Tucker *et al*., 2005). NDVI is resampled to the same spatial resolution of GPCC using the bilinear interpolation method. Table 7 displays that the NDVI of MAM and JJA are positively correlated with the precipitation and it is significant at 99% confidence level for JJA (CC=0.57, $p<0.01$). Negative correlations are

Table 7 Correlation coefficient (CC) results between the seasonal precipitation and temperature during the three periods, and between the seasonal precipitation and the normalized difference vegetation index (NDVI) during 1982–2012, where the CC values are obtained by the linear least square method and ** significant at a 99% confidence level by student's t test

Variable	Period	MAM	JJA	SON	DJF
Temperature	1901–2013	–0.06	–0.24	0.15	0.27
	1951–2013	–0.13	–0.15	0.01	0.1
	1979–2013	–0.05	–0.13	–0.17	0.14
NDVI	1982–2012	0.18	0.57**	–0.32	–0.01

detected for SON and DJF. Furthermore, strong positive correlations are found between MAM precipitation and JJA NDVI (CC=0.65, $p<0.01$), and between JJA precipitation and SON NDVI (CC=0.49, $p<0.01$) which indicates the time lags of the influence of the precipitation on NDVI. These results suggested that the vegetation NDVI in Central Asia is mainly controlled by the precipitation during 1982–2012. The increasing precipitation and warming temperature of MAM and JJA provide favorable water-heat condition to improve the vegetation over Central Asia.

5 Conclusions

The evolutions of the seasonal precipitation of Central Asia were comprehensively analyzed during the last century based on the latest global monthly precipitation dataset GPCC V7. The spatiotemporal features of the seasonal precipitation were discussed using the linear least square method, EEMD method and EOF method. Furthermore, the relationships between the seasonal precipitation and ENSO over Central Asia were explored to reveal the influences of the ENSO on the seasonal precipitation variabilities. The ENSO-based composites of HGT, U- and V-wind field, and the total moisture fluxes and their divergences were analyzed to explain the possible physical mechanisms about the ENSO-related seasonal precipitation over Central Asia.

Among the four seasons, MAM and JJA have the main contribution to the annual precipitation with the largest precipitation in MAM (mean=59 mm) over Central Asia. For the last century (1901–2013), increasing trends are found in MAM and DJF with the rates of 0.41 mm/10a and 0.39 mm/10a, while decreasing trends are for JJA and SON. During 1951–2013, four seasons have the increasing precipitation with the largest trend in DJF (k=0.77 mm/10a). For 1979–2013, except the decreasing trend in SON, the other seasons have the increased precipitation, and the largest increasing trend appears in JJA (k=1.62 mm/10a). In addition, EEMD results show that the inter-annual signals with 3–7 years multi-periods are the dominant components for all the seasonal precipitation during 1901–2013. Compared with the entire region, the precipitation in the mountainous area has obvious seasonal variation in terms of the variability but also the change rates, relatively to that in the plain area.

Spatial distributions of the linear trends suggested that Xinjiang has been experienced the decreasing seasonal precipitation during 1901–2013 and increasing seasonal precipitation during 1951–2013. But for the period of 1979–2013, the spatial features of the linear trends over Xinjiang appear large difference with almost all positive trends in DJF. For CAS5, the linear trends of the four seasons have different spatial distributions during our study periods. But it is confirmed that over northern Kazakhstan the precipitation has positive trends in MAM and JJA and negative trends in SON and DJF during the last three decades (1979–2013). EOF results show that the spatial distribution of EOF-1 mode in JJA is different from those of the other seasons during 1901–2013 which may be caused by different climate systems.

Furthermore, the relationships between the seasonal precipitation and ENSO show that ENSO has significantly positive influence on the variations of the seasonal precipitation ($p<0.05$) except JJA during 1951–2013. The composite analysis results suggest that during El Niño, there are more precipitation than the normal ENSO and La Niña over most parts of Central Asia, especially over the middle southern region. Southwesterly water vapor flux from the Arabic Sea and Africa is the source of Central Asia precipitation during El Niño. These water vapor fluxes are mainly generated in Indian and North Atlantic Oceans. The corresponding ENSO-based composites illustrated the possible physical mechanisms about the ENSO-related seasonal precipitation over Central Asia.

Finally, the relationships between the seasonal precipitation and temperature show that negative correlation is found in JJA, and positive correlation is found in DJF which are agree with the result in Trenberth and Shea (2005). For the arid and semiarid region over Central Asia, the precipitation in MAM and JJA is one major controller on the vegetation growth.

Acknowledgments

We thank Prof. Deliang Chen from Department of Earth Sciences, University of Gothenburg, Prof. Jianfeng Li from Department of Geography, Hong Kong Baptist University, and Dr. Gang Yin from Xinjiang University for their assistance during this study.

References

Abatzoglou J, Rupp D, Mote P, 2014. Seasonal climate variability and change in the Pacific northwest of the United States. *Journal of Climate*, 27: 2125–2142.

Aizen V, Aizen E, Melack J *et al*., 1997. Climatic and hydrologic changes in the Tien Shan, Central Asia. *Journal of Climate*, 10: 1393–1404.

Aizen E, Aizen V, Melack M *et al*., 2001. Precipitation and atmospheric circulation patterns at mid-latitudes of Asia. *International Journal of Climatology*, 21: 535–556.

Becker A, Finger P, Meyer-Christoffer A *et al*., 2013. A description of the global land-surface precipitation data products of the Global Precipitation Climatology Centre with sample applications including centennial (trend) analysis from 1901–present. *Earth System Science Data*, 5: 71–99.

Berg P, Haerter J, Thejll P *et al*., 2009. Seasonal characteristics of the relationship between daily precipitation intensity and surface temperature. *Journal of Geophysical Research*, 114: D18102.

Bintanja R, Selten F, 2014. Future increase in Arctic precipitation linked to local evaporation and sea-ice retreat. *Nature*, 509: 479–482.

Brown C, 1998. Applied Multivariate Statistics in Geohydrology and Related Sciences. Berlin Heidelberg: Springer, 155–157.

Chen F, Huang W, Jin L *et al*., 2011. Spatiotemporal precipitation variations in the arid Central Asia in the context of global warming, *Science China Earth Sciences*, 54: 1812–1821.

Chen L, Dool H, Becker E *et al*., 2017. ENSO Precipitation and temperature forecasts in the North American multimodel ensemble: Composite analysis and validation. *Journal of Climate*, 30: 1103–1125.

Chiodi A, Harrison D, 2015. Global seasonal precipitation anomalies robustly associated with El Niño and La Niña Events: An OLR perspective. *Journal of Climate*, 28: 6133–6159.

Chou C, Chiang J, Lan C *et al*., 2013. Increase in the range between wet and dry season precipitation. *Nature Geoscience*, 6: 263–267.

Dai A, Fung I, Del Genio A, 1997. Surface observed global land precipitation variations during 1900–1988. *Journal of Climate*, 10: 2943–2962.

Dai A, Wigley T, 2000. Global patterns of ENSO-induced precipitation. *Geophysical Research Letters*, 27: 1283–1286.

Dai N, Arikin P, 2017. Twentieth century ENSO-related precipitation mean states in twentieth century reanalysis, reconstructed precipitation and CMIP5 models. *Climate Dynamics*, 48: 3061–3083.

De Luis M, Brunetti M, Gonzalez-Hidalgo J *et al*., 2010. Changes in seasonal precipitation in the Iberian Peninsula during 1946–2005. *Global and Planetary Change*, 74: 27–33.

De Luis M, Gonzalez-Hidalgo J, Longares L *et al*., 2009. Seasonal precipitation trends in the Mediterranean Iberian Peninsula in second half of 20th century. *International Journal of Climatology*, 29: 1312–1323.

Deflorio M, Pierce D, Cayan D *et al*., 2013. Western U.S. extreme precipitation events and their relation to ENSO and PDO in CCSM4. *Journal of Climate*, 15: 4231–4243.

Emerton R, Cloke H, Stephens E *et al*., 2017. Complex picture for likelihood of ENSO-driven flood hazard. *Nature Communications*, 8: 14796.

Feddersen, H., 2003. Predictability of seasonal precipitation in the Nordic region. *Tellus*, 55A: 385–400.

Han T, Wang H, Sun J, 2017. Strengthened relationship between eastern ENSO and summer precipitation over northeastern China. *Journal of Climate*, 30: 4497–4512.

Harris I, Jones P, Osborn T *et al*., 2014. Updated high-resolution grids of monthly climatic observations: The CRU TS3.10 Dataset. *International Journal of Climatology*, 34: 623–642.

Hoell A, Barlow M, Saini R, 2012. The leading pattern of intraseasonal and interannual Indian Ocean precipitation variability and its relationship with Asian circulation during the boreal cold season. *Journal of Climate*, 25: 7509–7526.

Hoell A, Barlow M, Cannon F *et al*., 2017. Oceanic origins of historical Southwest Asia precipitation during the boreal cold season. *Journal of Climate*, 30: 2885–2903.

Hoell A, Funk C, Barlow M, 2015. The forcing of Southwestern Asia teleconnections by low-frequency sea surface temperature variability during boreal winter. *Journal of Climate*, 28: 1511–1526.

Hu Z, 1997. Interdecadal variability of summer climate over East Asia and its association with 500 hPa height and global sea surface temperature. *Journal of Geophysical Research*, 102: 403–412.

Hu Z, Hu Q, Zhang C *et al*., 2016a. Evaluation of reanalysis, spatially-interpolated and satellite remotely-sensed precipitation datasets in Central Asia. *Journal of Geophysical Research–Atmospheres*, 121: 5648–5662.

Hu Z, Li Q, Chen X *et al*., 2016b. Climate changes in temperature and precipitation extremes in an alpine grassland of Central Asia. *Theoretical Applied Climatology*, 126: 519–531.

Hu Z, Yang S, Wu R, 2003. Long-term climate variations in China and global warming signals. *Journal of Geophysical Research*, 108(D19): 4614.

Hu Z, Zhang C, Hu Q *et al*., 2014. Temperature changes in Central Asia from 1979–2011 based on multiple datasets. *Journal of Climate*, 27: 1143–1167.

Hu Z, Zhou Q, Chen X *et al*., 2017. Variations and changes of annual precipitation in Central Asia over the last century. *International Journal of Climatology*, 37: 157–170.

Hu Z, Zhou Q, Chen X *et al*., 2018. Evaluation of three global gridded precipitation datasets in Central Asia based on rain gauge observations. *International Journal of Climatology*, doi: 10.1002/joc.5510.

Huang J, Ji M, Xie Y *et al*., 2016. Global semi-arid climate change over last 60 years. *Climate Dynamics*, 46: 1131–1150.

Hughes B, Saunders M, 2002. Seasonal prediction of European spring precipitation from El Niño-Southern Oscillation and local sea-surface temperatures. *International Journal of Climatology*, 22: 1–14.

Ji F, Wu Z, Huang J *et al*., 2014. Evolution of land surface air temperature trend. *Nature Climate Change*, 4: 462–466.

Jia X, Ge J, 2017. Interdecadal changes in the relationship between ENSO, EAWM, and the wintertime precipitation over China at the end of the twentieth century. *Journal of Climate*, 30: 1923–1936.

Knippertz P, Ulbrich U, Marques F *et al*., 2003. Decadal changes in the link between El Niño and springtime North Atlantic Oscillation and European–North African rainfall. *International Journal of Climatology*, 23: 1293–1311.

Li B, Chen Y, Chen Z *et al*., 2016. Why does precipitation in northwest China show a significant increasing trend from 1960 to 2010? *Atmospheric Research*, 167: 275–284.

Li Q, Chen Y, Shen Y *et al*., 2011. Spatial and temporal trends of climate change in Xinjiang, China. *Journal of Geographical Sciences*, 21: 1007–1018.

Lloyd-Hughes B, Saunders M A, 2002. Seasonal prediction of European spring precipitation from El Niño–Southern Oscillation and local sea-surface temperatures. *International Journal of Climatology*, 22: 1–14.

Lorenz E N, 1956. Empirical Orthogonal Functions and Statistical Weather Prediction. Statistical Forecast Project Rep. 1, MIT. Department of Meteorology, Cambridge, MA, 49 pp.

Mann M, 2011. On long range dependence in global surface temperature series. *Climatic Change*, 107: 267–276.

Maussion F, Scherer D, Molg T *et al*., 2014. Precipitation seasonality and variability over the Tibetan Plateau as resolved by the High Asia reanalysis. *Journal of Climate*, 27: 1910–1927.

Madden R A, Williams J, 1978. The correlation between temperature and precipitation in the United States and Europe. *Monthly Weather Review*, 106: 142–147.

Mariotti A, 2007. How ENSO impacts precipitation in southwest Central Asia. *Geophsical Research Letters*, 34: L16706.

New M, Todd M, Hulme M *et al*., 2001. Precipitation measurements and trends in the twentieth century. *International Journal of Climatology*, 21: 1899–1922.

Noake K, Polson D, Hegerl G *et al*., 2012. Changes in seasonal land precipitation during the latter twentieth-century. *Geophysical Research Letters*, 39: L03706.

Ouyang R, Liu W, Fu G *et al*., 2014. Linkages between ENSO/PDO signals and precipitation, stream flow in China during the last 100 years. *Hydrology and Earth System Sciences*, 18: 3651–3661.

Park S, 2004. Remote ENSO influence on Mediterranean sky conditions during late summer and autumn: Evidence for a slowly evolving atmospheric bridge. *Quarterly Journal of the Royal Meteorological Society*, 130: 2409–2422.

Poli P, Hersbach H, Dee D *et al*., 2016. ERA-20C: An atmospheric reanalysis of the twentieth century. *Journal of*

Climate, 29: 4083–4097.

Qian W, Kang H, Lee D, 2002. Distribution of seasonal rainfall in the East Asian monsoon region. *Theoretical and Applied Climatology*, 73: 151–168.

Ropelewski C, Halpert M, 1987. Global and regional scale precipitation patterns associated with the E1 Niño/Southern Oscillation. *Monthly Weather Review*, 115: 1606–1626.

Russo S, Sterl A, 2012. Global changes in seasonal means and extremes of precipitation from daily climate model data. *Journal of Geophysical Research*, 117: D01108.

Rudolph J, Friedrich K, 2013. Seasonality of vertical structure in radar-observed precipitation over southern Switzerland. *Journal of Hydrometeorology*, 14: 318–330.

Schiemann R, Chiemann L, Luthi D *et al*., 2008. The precipitation climate of Central Asia: Intercomparison of observational and numerical data sources in a remote semiarid region. *International Journal of Climatology*, 2: 295–314.

Schneider U, Becker A, Finger P *et al*., 2014. GPCC's new land surface precipitation climatology based on quality-controlled in situ data and its role in quantifying the global water cycle. *Theoretical and Applied Climatology*, 115: 15–40.

Schneider U, Becker A, Finger P *et al*., 2015. GPCC Full Data Reanalysis Version 7.0 at 0.5º: Monthly land-surface precipitation from rain-gauges built on GTS-based and historic data. doi: 10.5676/DWD_GPCC/FD_M_V7_050.

Shaman J, 2014. The seasonal effects of ENSO on European precipitation: Observational analysis. *Journal of Climate*, 27: 6423–6438.

Smith T, Arkin P, Ren L *et al*., 2012. Improved reconstruction of global precipitation since 1900. *Journal of Atmospheric and Oceanic Technology*, 29: 1505–1517.

Sorg A, Bolch T, Stoffel M, 2012. Climate change impacts on glaciers and runoff in Tien Shan (Central Asia). *Nature Climate Change*, 2: 725–731.

Trenberth K, Shea D, 2005. Relationships between precipitation and surface temperature. *Geophysical Research Letters*, 32: L14703.

Tucker C J, Pinzon J E, Brown M E *et al*., 2005. An extended AVHRR 8-km NDVI data set compatible with MODIS and SPOT vegetation NDVI data. *International Journal of Remote Sensing*, 26: 4485–5598.

Van Oldenborgh G, Burgers G, Tank A, 2000. On the El Niño teleconnection to spring precipitation in Europe. *International Journal of Climatology*, 20: 565–574.

Wang S, Huang J, He Y *et al*., 2014. Combined effects of the Pacific decadal oscillation and El Niño-southern oscillation on global land dry–wet changes. *Scientific Reports*, 4: 6651.

Wang Y, Yan Z, 2009. Trends in seasonal precipitation over China during 1961–2007. *Atmospheric and Oceanic Science Letters*, 2: 165–171.

Wang Y, Zhou L, 2005. Observed trends in extreme precipitation events in China during 1961–2001 and the associated changes in large-scale circulation. *Geophysical Research Letters*, 32: L09707.

Ward P, Jongman B, Kummu M *et al*., 2014. Strong influence of El Niño Southern Oscillation on flood risk around the world. *PNAS*, 111: 15659–15664.

Wu Z, Huang N, 2004. A study of the characteristics of white noise using the empirical mode decomposition method. *Proceedings of the Royal Society A*: *Mathematical, Physical and Engineering Sciences*, 460: 1597–1611.

Wu Z, Huang N, 2009. Ensemble empirical mode decomposition: A noise-assisted data analysis method. *Advance in Adaptive Data Analysis*, 1: 1–41.

Xiao M, Zhang Q, Singh V, 2015. Influences of ENSO, NAO, IOD and PDO on seasonal precipitation regimes in the Yangtze River basin, China. *International Journal of Climatology*, 35: 3556–3567.

Xu L G, Zhou H F, Du L *et al*., 2015. Precipitation trends and variability from 1950 to 2000 in arid lands of Central Asia. *Journal of Arid Land*, 7(4): 514–526.

Xie P, Arkin P, 1997. Global precipitation: A 17-year monthly analysis based on gauge observations, satellite estimates and numerical model outputs. *Bulletin of American Meteorological Society*, 78: 2539–2558.

Yatagai A, Kamiguchi K, Arakawa O *et al*., 2012. APHRODITE: Constructing a long-term daily gridded precipitation dataset for Asia based on a dense network of rain gauges. *Bulletin of American Meteorological Society*, 93: 1401–1415.

Zanchettin D, Franks S W, Traverso P *et al*., 2008. On ENSO impacts on European wintertime rainfalls and their modulation by the NAO and the Pacific multi-decadal variability described through the PDO index. *International Journal of Climatology*, 28: 995–1006.

Zhang Q, Xu C, Chen X *et al*., 2011. Statistical behaviours of precipitation regimes in China and their links with atmospheric circulation 1960–2005. *International Journal of Climatology*, 31: 1665–1678.

Zhao W, Khalil M A K, 1993. The relationship between precipitation and temperature over the contiguous United States. *Journal of Climate*, 6: 1232–1236.

Zveryaev I, 2004. Seasonality in precipitation variability over Europe. *Journal of Geophysical Research*, 109: D05103.